Modelling the Impact of the Stator Currents on Inductance-Based Sensorless Control of Brushless DC-Machines

Fabien Gabriel*§, Frederik De Belie†, Peter Sergeant‡ and Xavier Neyt*
*Signal and Image Centre (CISS), Royal Military Academy (RMA), Brussels, Belgium
†Dept Electrical Energy, Systems & Automation (EESA), Ghent University (UGent), Gent, Belgium
‡Dept Electrotechnology, Faculty of Applied Engineering Sciences, University College Ghent, Gent, Belgium
§phone: +32 2 742 66 65, e-mail: fgabriel@elec.rma.ac.be

***Abstract*—Inductance-based sensorless control methods allow to estimate the rotor position by tracking the magnetic anisotropy linked to the rotor, partly caused by the magnetic saturation of the iron. In most salient-pole machines, the magnetic field in the air-gap may be approached by a sinusoidal function along the air-gap. Furthermore, the stator self-inductance mainly varies with two times the electrical rotor angle. In brushless DC-machines however, inductance-based estimations are affected by an important harmonic content in the magnetic field. Besides, it is well-known that large stator currents cause position estimation errors due to a variable magnetic state. This paper proposes a simple analytical model to take into account the combined effects of the stator currents and the harmonics. The goal is to understand these effects on the position estimation through simulations. The model is specifically developed for surface-mounted permanent-magnet brushless DC-machines with diametric single-slot-pair windings. The results suggest that the combined effects could be used to compensate for the position estimation error.**

I. Introduction

Many machine closed-loop control schemes require the knowledge of the rotor position. Among these, the conventional control of the permanent-magnet (PM) brushless DC-machine (BLDC) requires the detection of the rotor position at specific positions in order to commutate the currents between phases and to maintain a constant torque [1], [2]. The position can be measured by dedicated sensors, such as hall-effect sensors in case of the BLDC-machine [3]. More and more, position estimation methods are used, measuring the terminal currents and voltages only. These last solutions, often referred to as sensorless methods, have the advantage to remove the expensive dedicated sensors and improve the reliability of the drive [2].

At low speed and standstill, sensorless methods based on the back-electromotive force yield inaccurate estimations [2]–[4]. To estimate the position, methods based on the magnetic anisotropy related to the rotor position can be used. The magnetic anisotropy is the variation of the magnetic properties depending on the angle along the air-gap. The sources of anisotropy can be either salient poles or variable local saturation levels in the iron [5]. The magnetic anisotropy results in variations in the stator incremental inductance, i.e. the link between small stator current variations and the small flux linkage variations, as a function of the rotor position.

In most AC machines, the conductor distribution and the magnetic field along the air-gap can be approached sinusoidally, with the pole pitch as period. Assuming this, the variations of the stator incremental inductances are directly related to the rotor position [6]. In brushless DC-machines however, the non-sinusoidal winding distribution and the trapezoidal shape of the magnetic field produce additional harmonic content in the magnetic anisotropy along the air-gap and, by consequence, in the flux linkage variations [7]. As these harmonics are neglected in sensorless methods, the variations of the stator incremental inductances result in a distorted estimation of the rotor position. This was previously analyzed for a surface mounted BLDC-machine with diametric single-slot-pair windings [8]. Small stator currents were assumed in order to neglect their impact on the magnetic state. As expected, the results showed a distortion in the position estimation. Nevertheless, the estimation error was negligible at the positions corresponding to the traditional commutation instants. This suggested that no correction to the position estimation was required in a no-load conventional control of the BLDC-machine.

Many papers discuss the influence of the stator currents on the stator inductance and the impact on the position error for sinusoidal magnetic field-distributions. An analytical model taking the stator currents source into account was proposed by [6]. Numerous papers revealed the position error through finite-element computations and experiments [9]–[12]. Many of them suggest to perform an offline identification of the error as a function of the stator current amplitude.

This paper attempts to give a simple analytical model of the anisotropy that takes into account the combined effects of the stator currents and the harmonics. The model is specifically developed for surface-mounted permanent-magnet brushless DC-machines with diametric single-slot-pair windings. This model is used to perform Matlab simulations. The simulation results are qualitatively analyzed and suggest the possibility to use the combined impact of harmonics and large stator currents in order to perform an online identification of the

This work is financed by the Belgian government as part of the Belgian Defense research program F0709. It is performed in collaboration with UGent in the framework of the *Interuniversity Attraction Poles* program IUAP P6/21. The UGent authors also wish to thank the *Research Foundation-Flanders* (FWO) for the financial support in the framework of project number G.0665.06.

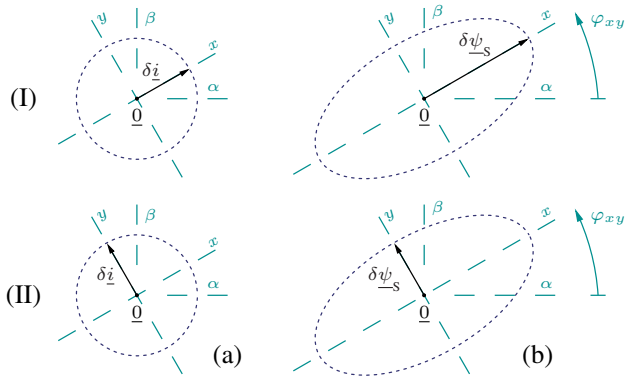

Fig. 1. Illustration of (b) $\delta\underline{\psi}_{\mathrm{S}}$ corresponding to (a) $\delta\underline{i}$ oriented following (I) the x-axis and (II) the y-axis of the xy-frame rotated by an angle φ_{xy} regarding the $\alpha\beta$ stator frame. The blue dashed lines represent the path drawn by the space vectors when $\delta\underline{i}$ rotates.

error due to the currents. The results are compared to some experimental measurements performed on a low inductance 3kW BLDC-machine using injection of voltage-adaptive test-pulses sequences [13].

II. The Inductance Model

A. Space vectors

The proposed inductance model is based on the concept of space vectors. In a $\alpha\beta$ reference-frame related to the stator, the space vectors result from the Clarke transformation applied to the phase variables [14]: $\underline{x} = C'X$, where $\underline{x}$ is the space vector, indicated by an underlined letter, corresponding to the phase values contained in X, and C' is the transformation matrix. Generally, the axis α is defined along an arbitrary first phase, numbered a in Fig. 3(b), and the axis β is defined in quadrature regarding α. The angle of a space vector $\mathrm{angle}(\underline{x})$ in the $\alpha\beta$ reference-frame is given from the direction α. Assuming a strict three phase machine, i.e. without neutral connection, we also have $X = C\underline{x}$, where C is such that $C'C = \mathbf{1}$.

This space-vector concept is generally used in machines where the magnetic field can be approached as a sinusoidal function along the air-gap, with one pole pitch as period. Nevertheless, the mathematical transformation is valid for any magnetic field function and is very convenient to simplify the number of equations for three-phase machines. In case of a non-sinusoidal magnetic field function however, the harmonics may affect the fundamental components as modelled by the space-vector theory.

B. The xy-frame

Let's define the space vector of small stator current variations $\delta\underline{i}$ and the space vector of their contribution to the flux $\delta\underline{\psi}_{\mathrm{S}}$. Note that $\delta\underline{i}$ can represent small variations due to the normal operating drive as well as the response to the injection of test signals. The relation between $\delta\underline{\psi}_{\mathrm{S}}$ and $\delta\underline{i}$ depends on the magnetic state of the machine. As illustrated in Fig. 1, in an anisotropic machine, an xy-frame can be defined such that the axes x and y are along the directions that correspond to the maximum and minimum amplitudes of $\delta\underline{\psi}_{\mathrm{S}}$ respectively, considering the angle of $\delta\underline{i}$ as variable. The orientation of the xy-frame regarding the stator reference-frame, noted φ_{xy}, is used as the estimator of the PM-rotor position φ_{PM}.

The advantage of using the xy-frame compared to the synchronous qd-frame fixed to the PM-rotor (where d is oriented along the axis of the PM, i.e. with an angle φ_{PM}) is that it ables to zero the magnetic cross-coupling effect that typically exist in the qd-frame [10], even with a sinusoidal magnetic field. The orientation of the xy-frame is however strongly affected by the harmonics and by large stator currents.

C. The incremental inductances using space vectors

It was discussed in [8] that the link between $\delta\underline{\psi}_{\mathrm{S}}$ and $\delta\underline{i}$ in the $\alpha\beta$ reference-frame can be written as

$$\delta\underline{\psi}_{\mathrm{S}} = l_C\delta\underline{i} + l_\Delta\delta\underline{i}^{*\angle 2\varphi_{xy}} \tag{1}$$

where $\delta\underline{i}^*$ is the inverse rotating current space vector such that $\mathrm{angle}(\delta\underline{i}^*) = -\mathrm{angle}(\delta\underline{i})$ and where $\angle 2\varphi_{xy}$ denotes a rotation of $2\varphi_{xy}$. The demonstration can be found in section VIII-A. If the PM-rotor position φ_{PM} and load currents $\underline{i}$ are not changing, the magnetic state of the machine is fixed. This results in constant values for the incremental inductances l_C, l_Δ and for the angle xy-frame angle φ_{xy}. When the magnetic state changes, these values may vary.

For convenience, we use a *delta inductance space vector* $\underline{l}_\Delta$ defined by:

$$\underline{l}_\Delta = \left(\delta\underline{\psi}_{\mathrm{S}} - l_C\delta\underline{i}\right)/\delta\underline{i}^* = l_\Delta\underline{1}_\alpha^{\angle 2\varphi_{xy}} \tag{2}$$

where $\underline{1}_\alpha$ is an unitary space vector oriented along α axis. This $\underline{l}_\Delta$ is easily computed from signal-injection based methods or other recent methods without additional signals-injection method such as in [15], and yields $\mathrm{angle}(\underline{l}_\Delta) = 2\varphi_{xy}$.

D. Computation from phase values

Assume we have the 3×3 stator incremental inductance matrix L that links the small phase-current variations δi_p to the small flux linkage variations $\delta\psi_{\mathrm{S},p'}$, $\forall p, p' \in \{a, c, b\}$:

$$L = \begin{bmatrix} l_{aa} & l_{ab} & l_{ac} \\ l_{ba} & l_{bb} & l_{bc} \\ l_{ca} & l_{cb} & l_{cc} \end{bmatrix} \tag{3}$$

such that

$$l_{p'p} = \frac{\partial\psi_{\mathrm{S},p'}}{\partial i_p} \tag{4}$$

The incremental inductance $\boldsymbol{l}$ of the relation using space vectors in the $\alpha\beta$ reference-frame, $\delta\underline{\psi}_{\mathrm{S}} = \boldsymbol{l}\delta\underline{i}$, is then computed by

$$\boldsymbol{l} = \begin{bmatrix} l_{\alpha\alpha} & l_{\alpha\beta} \\ l_{\beta\alpha} & l_{\beta\beta} \end{bmatrix} \equiv C'LC \tag{5}$$

where C and C' are the transformation matrix given in section II-A. Note that $l_{\alpha\beta} = -l_{\beta\alpha}$. From (1) and (5), it yields

$$l_C = \frac{l_{\alpha\alpha} + l_{\beta\beta}}{2} \quad \text{and} \quad \underline{l}_\Delta = (l_{\alpha\alpha} - l_C)\,\underline{1}_\alpha + l_{\alpha\beta}\underline{1}_\beta \tag{6}$$

The demonstration can be found in section VIII-B.

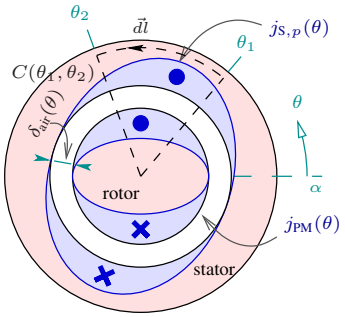

Fig. 2. Single-pole-pair representation of an electrical machine section with the current distribution $j_{S,p}(\theta)$ of the p-phase at the stator side (other phases are not illustrated here), and the current distribution $j_{PM}(\theta)$ corresponding to the PM of the rotor side.

The next section proposes an analytical model of the anisotropy. The model is developed for a simplified BLDC-machine model in order to compute the matrix L. The simulations and analysis of φ_{xy} as a function of φ_{PM} are based on that model.

III. The Analytical Anisotropy Model

A. General case

Fig. 2 illustrates the single-pole-pair representation of an electrical machine where θ is the electrical angle measured from the α-axis. On the stator side, the current distribution $j_{S,p}(\theta)$ due to the phase p is given by the conductor distribution $n_{S,p}(\theta)$ multiplied by the current intensity i_p flowing in that phase:

$$j_{S,p}(\theta) = i_p n_{S,p}(\theta) \tag{7}$$

On the rotor side, assume that the permanent magnets can be approached by an equivalent current distribution $j_{PM}(\theta)$. Summing the contribution of the permanent-magnets and the stator phases, the total current distribution is written

$$j_{total}(\theta) = j_{PM}(\theta) + \sum_p j_{S,p}(\theta, i_p) \tag{8}$$

Assume also that the conductivity of the iron is zero and that the magnetic field in the air-gap is strictly radial $\vec{H}|_{air} = H\vec{1}_r$.

The Ampere's law computed on a closed path $C(\theta_1, \theta_2)$ crossing the air-gap at any angles θ_1 and θ_2, as illustrated in Fig. 2, yields

$$\oint_{C(\theta_1,\theta_2)} \vec{H} \cdot \vec{dl} = \int_{\theta_1}^{\theta_2} j_{total}(\theta) d\theta \tag{9}$$

where $\vec{dl}$ is the contour element vector. Let's write the right part of the Ampere's law by defining the magnetomotive force distribution $F_{total}(\theta)$:

$$F_{total}(\theta_2) - F_{total}(\theta_1) = \int_{\theta_1}^{\theta_2} j_{total}(\theta) d\theta \tag{10}$$

Using (8), we can write $F_{total}(\theta_2)$ as the result of the contribution of each current distribution to the magnetomotive force:

$$F_{total}(\theta) = F_{PM}(\theta) + \sum_p F_{S,p}(\theta, i_p) \tag{11}$$

where each contribution is computed alone using (10) and assuming $\oint_{2\pi} F(\theta) d\theta = 0$. Here, we can define the *embraced surface* distribution $N_{S,p}(\theta)$ of the phase p:

$$N_{S,p}(\theta_2) - N_{S,p}(\theta_1) = \int_{\theta_1}^{\theta_2} n_{S,p}(\theta) d\theta \tag{12}$$

where assume $\oint_{2\pi} N(\theta) d\theta = 0$. Therefore, (11) can be written:

$$F_{total}(\theta) = F_{PM}(\theta) + \sum_p i_p N_{S,p}(\theta, i_p) \tag{13}$$

In order to compute the left part of the Ampere's law (9), we must discuss the magnetic anisotropy. This anisotropy is caused either by the variation of the air-gap length $\delta_{air}(\theta)$, generally from the rotor side. Or by the local saturation level in the iron, resulting in a reduction of the iron permeability. Assume that this permeability reduction mainly occurs close to the surface and that it can be transposed in an ideal machine, i.e. having an infinite iron permeability [1], as an equivalent expansion of the air-gap length $\delta_{iron}(|F_{total}|)$ depending on the total magnetomotive force amplitude $|F_{total}|$ at the considered angle. Eq. (9) yields

$$\Big(\delta_{air}(\theta) + \delta_{iron}(|F_{total}|)\Big) H(\theta) = F_{total}(\theta) \tag{14}$$

where $\delta_{air} > 0$ and $\delta_{iron} \geq 0$. The magnetic induction in the air-gap is then $B(\theta) = \mu_0 H(\theta)$, where μ_0 is the air permeability. Note that these assumptions mainly neglect the saturation that may occur deeper in the core of the stator and in the rotor, and that they do not take into account the azimuthal component of the field in the air-gap. These are strong approximations. However, it gives satisfying results for the considered analysis.

Finally, it can be shown that the flux linked by the phase p' is [16]:

$$\psi_{S,p'} = l_m R_S \oint_{2\pi} N_{S,p'}(\theta) B(\theta) d\theta \tag{15}$$

where l_m is the machine length and R_S is the radius to the air-gap surface.

From these equations, we can extract the relationship between the phase currents i_p and the flux linkages $\psi_{S,p'}$ in any anisotropic machine, assuming that the saturation mainly occurs close to the rotor surface.

B. Model assuming small variations

Since we are interested in the incremental inductances, defined in (4), let's fist calculate the partial derivative of $H(\theta)$:

$$\frac{\partial H(\theta)}{\partial i_{p'}} = \frac{dH(\theta)}{dF_{total}} \frac{\partial F_{total}}{\partial i_{p'}} \tag{16}$$

From (13), we have:

$$\frac{\partial F_{total}(\theta)}{\partial i_{p'}} = N_{S,q}(\theta) \tag{17}$$

We define the anisotropy factor distribution that carries the incremental effect of the anisotropy by:

$$k_{ani}(\theta, F_{total}) = \delta_0 \frac{dH(\theta)}{dF_{total}} \tag{18}$$

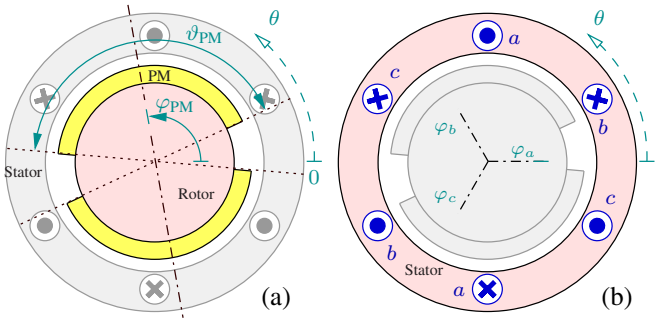

Fig. 3. Section of the BLDC-machine showing the rotor structure with its PM (a), and the stator structure with its phase conductor slots (b)

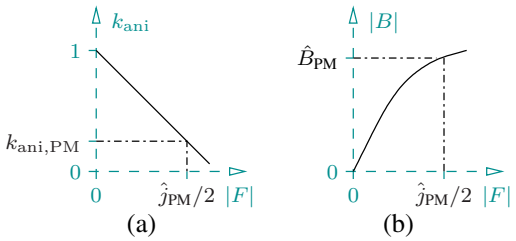

Fig. 4. (a) Proposed anisotropy function $k_{\mathrm{ani}}(|F|)$; (b) Illustration of the magnetizing curve $B(|F|)$

where δ_0 is any arbitrary value, for example the minimum real air-gap length. This anisotropy factor k_{ani} is equal to 1 if there is no saturation: $\delta_{\mathrm{iron}} = 0$; and if $\delta_{\mathrm{air}}(\theta) = \delta_0$. It decrease while the saturation increases. This anisotropy factor distribution is computed using (14). Introducing (17) and (18), (16) yields

$$\frac{\partial H(\theta)}{\partial i_p} = \frac{k_{\mathrm{ani}}(\theta, F_{\mathrm{total}})}{\delta_0} N_{\mathrm{S},p}(\theta) \tag{19}$$

Using (15) in (19), we can compute the phase incremental inductance $l_{p'p}$ as given in (4):

$$l_{p'p} = l_m R_{\mathrm{S}} \frac{\mu_0}{\delta_0} \oint_{2\pi} k_{\mathrm{ani}}(\theta, F_{\mathrm{total}}) N_{\mathrm{S},p'}(\theta) N_{\mathrm{S},p}(\theta) d\theta \tag{20}$$

The machine design parameters (δ_{air}, $N_{\mathrm{S},p}$, F_{PM}) and the the saturation behaviour (δ_{iron}) are given hereafter for a Brushless DC-machine with diametric single-slot-pair windings.

C. BLDC-machine design

Consider a three-phase single-pole-pair surface-mounted permanent-magnet brushless DC-machine with constant air-gap length $\delta_{\mathrm{air}}(\theta) = \delta_0$. As illustrated in Fig. 3(a), the axis of the PM forms an angle φ_{PM} with respect to the angular position $\theta = 0$ and each PM covers a magnet-pole angle ϑ_{PM}. Assume that the PM can be approach by currents $\hat{\jmath}_{\mathrm{PM}}$ located at the ends of the magnets, the equivalent magnetomotive force distribution is therefore:

$$F_{\mathrm{PM}}(\theta) = \begin{cases} +\hat{\jmath}_{\mathrm{PM}}/2 & \text{if } \theta \in [\varphi_{\mathrm{PM}} - \frac{\vartheta_{\mathrm{PM}}}{2}, \varphi_{\mathrm{PM}} + \frac{\vartheta_{\mathrm{PM}}}{2}] \\ -\hat{\jmath}_{\mathrm{PM}}/2 & \text{if } \theta \in [\varphi_{\mathrm{PM}} - \pi + \frac{\vartheta_{\mathrm{PM}}}{2}, \varphi_{\mathrm{PM}} - \pi - \frac{\vartheta_{\mathrm{PM}}}{2}] \\ 0 & \text{otherwise} \end{cases} \tag{21}$$

As illustrated in Fig. 3(b), the diametric single-slot-pair windings of each phase, labeled by $p \in \{a, b, c\}$, are wound with $\hat{N}$ conductor turns around the phase axis defined by $\varphi_a = 0$, $\varphi_b = \frac{2\pi}{3}$ and $\varphi_c = \frac{4\pi}{3}$, and located at the positions $\varphi_p - \pi/2$ and $\varphi_p + \pi/2$. The embraced surface distribution of a phase p is therefore:

$$N_{\mathrm{S},p}(\theta) = \begin{cases} +\hat{N}/2 & \text{if } \theta \in [\varphi_p - \frac{\pi}{2}, \varphi_p + \frac{\pi}{2}] \\ -\hat{N}/2 & \text{if } \theta \in [\varphi_p + \frac{\pi}{2}, \varphi_p - \frac{\pi}{2}] \end{cases} \tag{22}$$

The detail of the development of the expression of $l_{p'p}$ for that BLDC-machine using these parameters can be found in the appendix of [8].

D. The anisotropy function

In order to perform simple simulations based on the proposed machine anisotropy model, we assume a simplified anisotropy function $k_{\mathrm{ani}}(|F|)$ that varies linearly between an unsaturated point where $k_{\mathrm{ani}} = 1$ and a given saturated point $k_{\mathrm{ani}} = k_{\mathrm{ani,PM}}$, as illustrated in Fig. 4(a). The reference for this saturation point corresponds to the value of the saturation due to the PM magnetomotive force only, under the PM. As we do not have physically access to this values in a real machine, we made adjustments such that the magnitudes of the simulated inductances are similar to the experimental results.

From $k_{\mathrm{ani}}(|F|)$ and assuming $\delta_{\mathrm{air}}(\theta) = \delta_0$, we can deduce the relation between B and F using (16) and (18). An illustration is given in Fig. 4(b). Assuming the simplified anisotropy function, this relation is of the second order. For the considered range, this approximation curve is satisfying.

IV. Simulation Results

A. Simulation data

The design parameters used for the Matlab simulations correspond to the experimental machine. They are:

Machine length l_m	7.1 cm
Stator radius R_S	12 cm
Air-gap length δ_0	5 mm
Pair-pole number n_{pp}	14
PM-rotor pole angle ϑ_{PM}	0.85π
Conductor turns $\hat{N}$	4

The following magnetic parameters are assumed:

peak air-gap PM induction $\hat{B}_{\mathrm{PM}}$	0.6 T
anisotropy factor under the PM $k_{\mathrm{ani,PM}}$	0.25

The simulations neglect the magnetic fields at the axial ends, the azimuthal magnetic field in the air-gap, the air-gap variations due to the teeth and the saturation in the stator and rotor cores.

The stator currents are set in quadrature regarding the PM orientation, i.e. $\underline{i} = i\underline{1}_q$. This corresponds to the field oriented control of most of the PM synchronous machines. This is not the conventional control of a BLDC-machine, but it allows to observe the inductance-base position estimation throughout the whole revolution of the stator current space vector.

B. Results

Fig. 5, Fig. 6 and Fig. 7 show:

(a) the space vector of the stator load currents $\underline{i}$;
(b) the plot of the delta inductance $\underline{l}_\Delta$ computed using the analytical model of the BLDC-machine;
(c) the inductance-base PM-rotor estimation angle $\varphi_{xy}+90^\circ$ as a function of the PM-rotor angle $\varphi_{\rm PM}$, computed using $2\varphi_{xy} = \text{angle}(\underline{l}_\Delta)$;
(d) the inductance $l_\Delta = |\underline{l}_\Delta|$ as a function of the PM-angle;
(e) the inductance l_C as a function of the PM-angle computed using the analytical model of the BLDC-machine;

1) No load simulation: Fig. 5 shows the simulation results with $\underline{i} = 0$. We see that $\underline{l}_\Delta$ draws a triangle shape during the rotation and that the inductance-based angle $\varphi_{xy} + 90^\circ$ gives a distorted estimation of the PM-positions $\varphi_{\rm PM}$. These results suggest that the inductance-based angle is not a continuous reliable estimation of the PM-rotor position throughout the revolution. In the conventional control of the BLDC-machine however, only specific position detections are required: the PM-positions $\varphi_{\rm PM}$ where the commutation of the currents should occur are located in zones around the angles $\varphi_{\rm PM} = 30^\circ + k60^\circ$ with an amplitude of allowed error $\pm(120^\circ - \vartheta_{\rm PM})/2$. If the currents commutate in these zones, the electrical torque should remain approximately constant. These zones are illustrated by dotted circles in Fig. 5(c). Assuming very small stator currents, they correspond to the inductance-based positions $\varphi_{xy} + 90^\circ = 30^\circ + k60^\circ$ and to the maximums of l_Δ.

2) Small load simulation: Fig. 6 shows the simulation results with a small stator current of amplitude $i = 12$A. We see that the triangle shape drawn by $\underline{l}_\Delta$ is slightly distorted and rotated. Let's define $\varphi_{\rm err}$ as the additional error of $\varphi_{xy} + 90^\circ$ compared to the no load results. In a sensorless control, this error could be identified at the position of the maximum amplitude of l_Δ by the rotation of $\underline{l}_\Delta$: here $2.57^\circ = 5.13^\circ/2$. However, the error is not constant throughout the revolution. This must be taken into account in a sensorless control as it can reduce the performance.

3) Large load simulation: Fig. 7 shows the simulation results with a large stator current amplitude, $i = 60$A. This is half the nominal value of the machine. The triangle shape and the inductance-based angle are even more distorted. The error at the maximum amplitude of l_Δ is here $10.77^\circ = 21.54^\circ/2$. However the error is even more variable throughout the revolution.

V. Experiments

A. Experimental set-up

The experimental BLDC-machine is a 3kW in-wheel motor with outer rotor developed by *Technicréa*, France, for the propulsion of small vehicles. The nominal stator current in the machine is 134A. Information about the design can be found in [17]. The machine is fed with an IGBT voltage-source inverter from *SEMIKRON* connected to a DC voltage rectifier. Low DC-voltage of about 50V is used to limit the amplitude of the currents ripples. The PWM generator works at 10kHz. Using such a low DC voltage and high switching periods reveals important nonlinearities in the inverter. Those nonlinearities are taken into account as discussed in [18], [19].

The machine rotates at an electrical frequency of 14Hz, that is about 10% of the rated speed. In order to keep the rotation speed as constant as possible, an encoder feedback is used in a field-oriented control drive. To estimate the inductance, test-pulses are injected every 8 switching periods in addition to the normal operating voltage. The resulting high-frequency current response is extracted from the current sensor measurements and used to calculate the inductance. The set-point for test current amplitude $|\delta\underline{i}|$ is 2A. This small amplitude is selected in order to neglect the impact of the test on the magnetic state and on the losses in the machine [20].

Note that experimental results with the unloaded machine were previously discussed in [19].

B. Measurements

Fig. 8 shows the experimental results with a small stator current of amplitude $i \approx 11.5$A. Results are:

(a) the space vector of the stator load currents $\underline{i}$;
(b) the plot of the delta inductance $\underline{l}_\Delta$ computed from the test-pulses injection;
(c) the inductance-base PM-rotor estimation angle $\varphi_{xy}+90^\circ$ as a function of the PM-rotor angle $\varphi_{\rm PM}$, computed using $2\varphi_{xy} = \text{angle}(\underline{l}_\Delta)$;
(d) the inductance $l_\Delta = |\underline{l}_\Delta|$ as a function of the PM-angle;

The inductance l_C is assumed constant and is assessed on one PM-turn. No measurement is taken for $\underline{i}$ arround the angles $30^\circ + k60^\circ$. This is due to the inverter nonlinearities, as explained in [18]. The experimental results are in good correspondence with the simulations: as expected, the triangle shape drawn by $\underline{l}_\Delta$ is slightly rotated. The exact rotation angle is however difficult to estimate in that experiment due to important measurements noise. Moreover, due to the inverter nonlinearities, the test-pulse method is stopped during short periods of time, leaving some zones of the PM-angle without inductance-based angle estimations. To compensate for these problems, filtering would be required and an improved compensation of the inverter nonlinearities should be used.

VI. Observations for the Sensorless

The triangle shape drawn by $\underline{l}_\Delta$ during the PM rotation is due to the presence of the different harmonics in the anisotropic distribution. This result in a distorted inductance-base PM-angle estimation. The simulation and experimental results show that the stator currents produce an additional distortion on the estimation. The error due to this additional distortion regarding the no-load distortion seems not to be constant around the PM-rotation. Nevertheless, if this error can be approximatively rated, inductance-base PM-angle estimation could still be used in control methods that do not require an accurate position estimation, such as the conventional one. Strong degradation of the drive performances must however be considered.

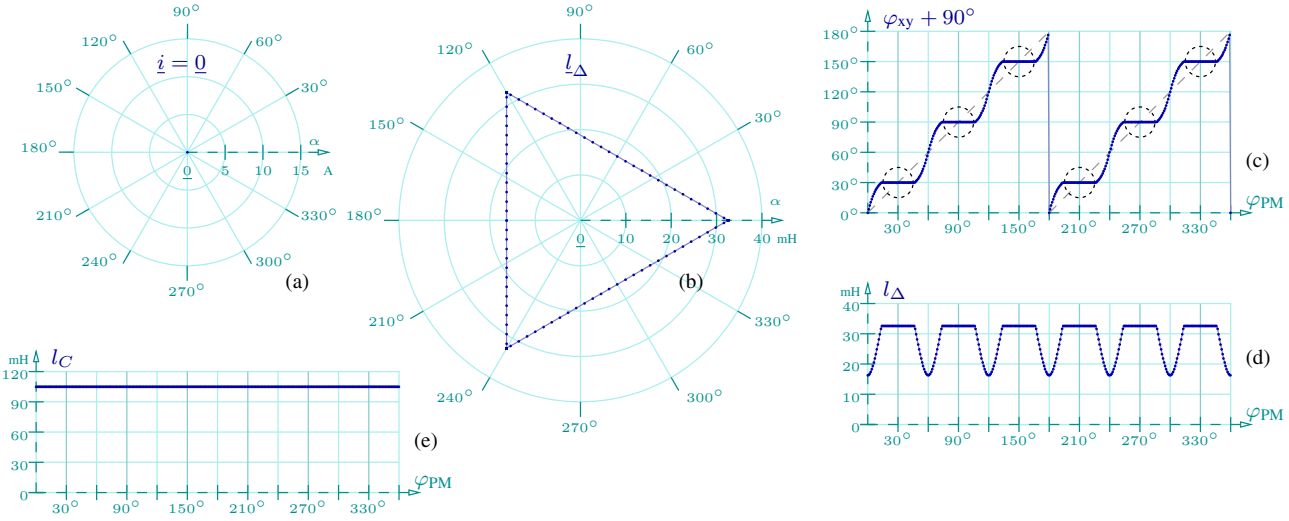

Fig. 5. Simulated values for one turn $\varphi_{PM} = [0° \rightarrow 360°]$ with (a) $\underline{i} = 0$.

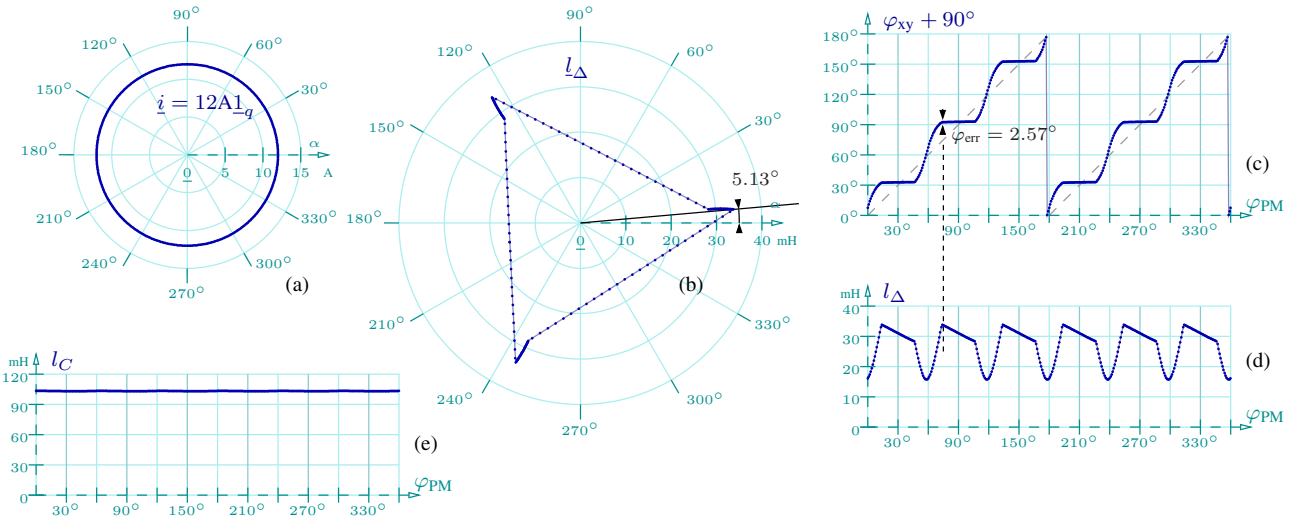

Fig. 6. Simulated values for one turn $\varphi_{PM} = [0° \rightarrow 360°]$ with (a) $\underline{i} = 12\text{A}\ \underline{1}_q$.

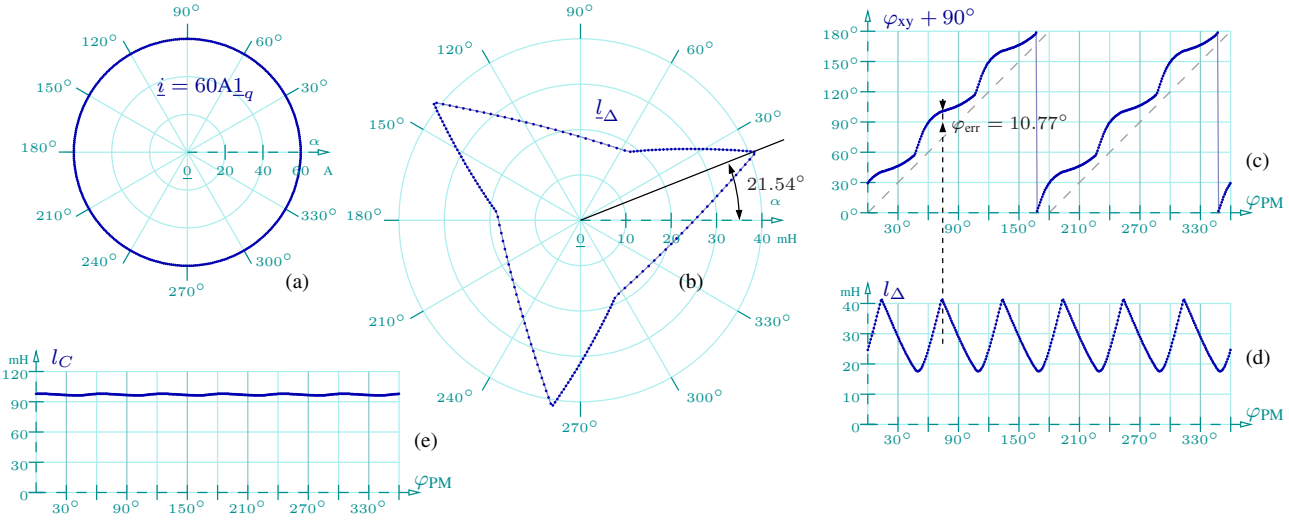

Fig. 7. Simulated values for one turn $\varphi_{PM} = [0° \rightarrow 360°]$ with (a) $\underline{i} = 60\text{A}\ \underline{1}_q$.

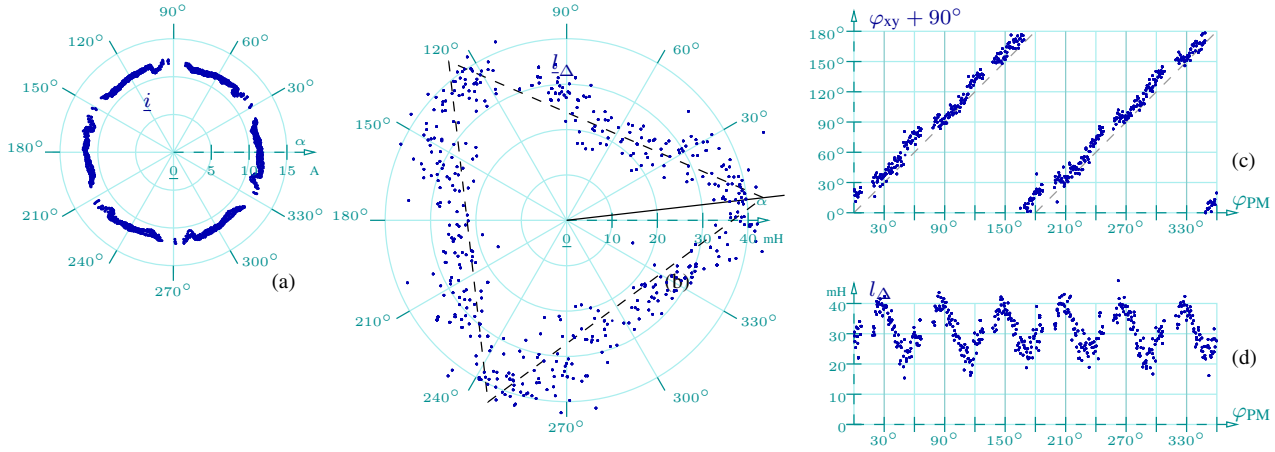

Fig. 8. Experimental values for one turn $\varphi_{\mathrm{PM}} = [0° \rightarrow 360°]$. $|\underline{i}| \approx 11.5$A. $l_C \approx 110\mu$H

Mainly from the simulation results, the rotation of the triangle-shape drawn by $\underline{l}_\Delta$ during the PM rotation seems to be related to the additional inductance-base angle estimation error due to the stator currents. This must be verified with further experiments at low and high load currents. If confirmed, this relationship would give a tool to identify the additional error online without any dedicated sensor.

VII. Conclusions and Futur Works

This paper proposed a simple analytical model to take into account the combined effects of the stator currents and the harmonics of the anisotropy distribution. The goal was to give a tool in order to understand these effects on the position estimation through simulations. The paper specifically focusses on surface-mounted permanent-magnet brushless DC-machines with diametric single-slot-pair windings.

The simulations revealed that the harmonics result in a distorted estimation of the PM-angle using the inductance-base position estimation method. This effect is amplified by large stator currents. Nevertheless, the simulations suggest that the additional distortion error due to stator currents could be identified through the harmonic effects on the inductance.

These simulations will further be complemented with experimental measurements and finite-element simulations. Further research should focus on the impact of the inductance-base PM-angle estimation error on the machine control drive performances.

VIII. Appendix

A. The incremental inductances using space vectors

Assume we initially have the following relation :

$$\delta\underline{\psi}_{\mathrm{S}} = \boldsymbol{l}\delta\underline{i} \tag{23}$$

where $\boldsymbol{l}$ is the incremental inductance using space vectors. Using the coordinates in the $\alpha\beta$ reference-frame, it yields

$$\begin{bmatrix} \delta\psi_{\mathrm{S},\alpha} \\ \delta\psi_{\mathrm{S},\beta} \end{bmatrix} = \begin{bmatrix} l_{\alpha\alpha} & l_{\alpha\beta} \\ l_{\alpha\beta} & l_{\beta\beta} \end{bmatrix} \begin{bmatrix} \delta i_\alpha \\ \delta i_\beta \end{bmatrix} \tag{24}$$

where $l_{\alpha\beta} = l_{\beta\alpha}$. This can be rewritten as :

$$\begin{bmatrix} \delta\psi_{\mathrm{S},\alpha} \\ \delta\psi_{\mathrm{S},\beta} \end{bmatrix} = \begin{bmatrix} \frac{l_{\alpha\alpha}+l_{\beta\beta}}{2} & 0 \\ 0 & \frac{l_{\alpha\alpha}+l_{\beta\beta}}{2} \end{bmatrix} \begin{bmatrix} \delta i_\alpha \\ \delta i_\beta \end{bmatrix} + \begin{bmatrix} \frac{l_{\alpha\alpha}-l_{\beta\beta}}{2} & -l_{\alpha\beta} \\ l_{\alpha\beta} & \frac{l_{\alpha\alpha}-l_{\beta\beta}}{2} \end{bmatrix} \begin{bmatrix} \delta i_\alpha \\ -\delta i_\beta \end{bmatrix} \tag{25}$$

We define :

$$\begin{cases} l_C = \frac{l_{\alpha\alpha}+l_{\beta\beta}}{2} \\ l_\Delta \cos(2\varphi_{xy}) = \frac{l_{\alpha\alpha}-l_{\beta\beta}}{2} \\ l_\Delta \sin(2\varphi_{xy}) = l_{\alpha\beta} \end{cases} \tag{26}$$

Therefore, it yields

$$\begin{bmatrix} \delta\psi_{\mathrm{S},\alpha} \\ \delta\psi_{\mathrm{S},\beta} \end{bmatrix} = l_C \begin{bmatrix} \delta i_\alpha \\ \delta i_\beta \end{bmatrix} + l_\Delta \begin{bmatrix} \cos(2\varphi_{xy}) & -\sin(2\varphi_{xy}) \\ \sin(2\varphi_{xy}) & \cos(2\varphi_{xy}) \end{bmatrix} \begin{bmatrix} \delta i_\alpha \\ -\delta i_\beta \end{bmatrix} \tag{27}$$

Using the space vectors, we have :

$$\delta\underline{\psi}_{\mathrm{S}} = l_C\delta\underline{i} + l_\Delta\delta\underline{i}^{*\angle 2\varphi_{xy}} \tag{28}$$

B. Computation from phase values

The delta inductance space vector $\underline{l}_\Delta$ is defined by (2) and is:

$$\underline{l}_\Delta = l_\Delta \underline{1}_\alpha^{\angle 2\varphi_{xy}} = l_\Delta \cos(2\varphi_{xy})\underline{1}_\alpha + l_\Delta \sin(2\varphi_{xy})\underline{1}_\beta \tag{29}$$

Using (26), it yields:

$$\underline{l}_\Delta = \frac{l_{\alpha\alpha} - l_{\beta\beta}}{2}\underline{1}_\alpha + l_{\alpha\beta}\underline{1}_\beta \tag{30}$$

References

[1] J. Chiasson, *Modeling and high performance control of electric machines*. USA: IEEE Computer Society Press, 2005.

[2] P. Acarnley and J. Watson, "Review of position-sensorless operation of brushless permanent-magnet machines," *IEEE Transactions on Industrial Electronics*, vol. 53, pp. 352 – 362, Apr. 2006.

[3] T.-H. Kim, H.-W. Lee, and M. Ehsani, "State of the art and future trends in position sensorless brushless dc motor/generator drives," in *Industrial Electronics Society Conference (IECON)*, pp. 1718 – 1725, Nov. 2005.

[4] J. Holtz, "Sensorless control of induction machines - with or without signal injection ?," *IEEE Transactions on Industrial Electronics*, vol. 53, pp. 7 – 30, Feb. 2006.

[5] O. Scaglione, M. Markovic, and Y. Perriard, "Exploitation of a new iron b-h phenomenon for the standstill position detection of pm motors," in *International Conference on Electrical Machines (ICEM)*, Sept. 2010.

[6] F. D. Belie, J. Melkebeek, K. Geldhof, L. Vandevelde, and R. Boel, "A general description of high-frequency position estimators for interior permanent-magnet synchronous motors," in *International Conference on Electrical Machines (ICEM)*, Sept. 2004.

[7] H.-W. Lee, T.-H. Kim, and M. Ehsani, "Power density maximization of the brushless dc generator," in *IEEE Annual Conference of Industrial Electronics Society (IECON)*, vol. 3, pp. 2162 – 2166, Nov. 2003.

[8] F. Gabriel, F. D. Belie, P. Druyts, and X. Neyt, "Sensorless drive of surface mounted permanent-magnet brushless dc machines with concentrated windings based on inductance measurements," in *IEEE International Conference on Power Electronics (ICPE'11) - ECCE Asia*, (Jeju, Korea), pp. 1236 – 1243, May 2011.

[9] L. Chedot and G. Friedrich, "A cross saturation model for interior permanent magnet synchronous machine. application to a starter-generator," in *IEEE Annual Meeting on Industry Applications*, vol. 1, Oct. 2004.

[10] P. Guglielmi, M. Pastorelli, and A. Vagati, "Cross-saturation effects in ipm motors and related impact on sensorless control," *IEEE Transactions on Industry Applications*, vol. 42, pp. 1516 – 1522, Nov. 2006.

[11] Y. Li, Z. Zhu, D. Howe, and C. Bingham, "Modeling of cross-coupling magnetic saturation in signal-injection-based sensorless control of permanent-magnet brushless ac motors," *IEEE Transactions on Magnetics*, vol. 43, pp. 2552 – 2554, June 2007.

[12] N. Bianchi, S. Bolognani, J.-H. Jang, and S.-K. Sul, "Comparison of pm motor structures and sensorless control techniques for zero-speed rotor position detection," *IEEE Transactions on Power Electronics*, vol. 22, pp. 2466 – 2475, Nov. 2007.

[13] F. De Belie, P. Sergeant, and J. Melkebeek, "A sensorless drive by applying test pulses without affecting the average-current samples," *IEEE Transactions on Power Electronics*, vol. 25, no. 4, pp. 875 – 888, 2010.

[14] P. Vas, *Electrical Machines and Drives: A Space-Vector Theory Approach*. United States: Oxford University Press, 1993. From inter-universitary loan.

[15] P. R. P. E. in a Direct-Torque Controlled Salient-Pole PMSM without Using Additional Test Signals, "Frederik de belie and thomas vyncke and jan melkebeek," in *International Conference on Electrical Machines (ICEM)*, pp. 1 – 6, Sept. 2010.

[16] W. Wang, K. Nam, and S. young Kim, "Concentric winding bldc motor design," in *IEEE International Conference on Electric Machines and Drives*, pp. 157 – 161, May 2005.

[17] H. Mai, F. Dubas, D. Chamagne, and C. Espanet, "Optimal design of a surface mounted permanent magnet in-wheel motor for an urban hybrid vehicle," in *IEEE Vehicle Power and Propulsion Conference (VPPC)*, pp. 481 – 485, 2009.

[18] F. Gabriel, F. D. Belie, P. Druyts, X. Neyt, J. Melkebeek, and M. Acheroy, "Compensating the influence of the stator resistor and inverter nonlinearities in signal-injection based sensorless strategies," in *IEEE Vehicle Power and Propulsion Conference (VPPC'09)*, (Dearborn, USA), pp. 283 – 290, Sept. 2009.

[19] F. Gabriel, F. D. Belie, P. Druyts, and X. Neyt, "Strategy to detect and prevent the current zero-crossing for inverter powered drives," in *IEEE International Conference on Electrical Machines (ICEM'10)*, (Rome, Italy), Sept. 2010.

[20] P. Sergeant, F. De Belie, L. Dupre, and J. Melkebeek, "Losses in sensorless controlled permanent-magnet synchronous machines," *IEEE Transactions on Magnetics*, vol. 46, pp. 590 – 593, Feb. 2010.